Research paper

Computer-aided drug discovery of Myc-Max inhibitors as potential therapeutics for prostate cancer

Lavinia A. Carabet [a], [1], Nada Lallous [a], [1], Eric Leblanc [a], Fuqiang Ban [a], Helene Morin [a], Sam Lawn [a], Fariba Ghaidi [a], Joseph Lee [a], Ian G. Mills [b], [c], Martin E. Gleave [a], Paul S. Rennie [a], [2], Artem Cherkasov [a], [*], [2]

[a] Vancouver Prostate Centre, University of British Columbia, 2660 Oak Street, Vancouver, British Columbia, V6H 3Z6, Canada
[b] Centre for Cancer Research and Cell Biology, Queen's University, Belfast, United Kingdom
[c] Nuffield Department of Surgical Sciences, John Radcliffe Hospital, University of Oxford, Oxford, United Kingdom

ARTICLE INFO

ABSTRACT

While Myc is an essential regulator of growth in normal cells, it is also frequently associated with cancer progression, therapy-resistance and lethal outcomes in most human cancers. In prostate cancer (PCa), Myc transcription factors are implicated in the pathogenesis and progression of the full spectrum of PCa, from adenocarcinoma to advanced castration-resistant and neuroendocrine phenotypes. Though a high-value therapeutic target, clinically approved anti-Myc drugs have yet to be discovered. To elicit its oncogenic effects, Myc must form a heterodimer with its partner Max, which together bind DNA and activate transcription of a spectrum of target genes that promote cell growth, proliferation, metabolism, and apoptosis while blocking differentiation. In this study, we identified a binding site on the DNA-binding domain of the structurally ordered Myc-Max complex and employed a computer-aided rational drug discovery approach to identify small molecules that effectively inhibit Myc-Max functionality. A large-scale virtual screening protocol implementing structure-based methodologies was utilized to select a set of top-ranked compounds that were subsequently evaluated experimentally and characterized mechanistically for their ability to inhibit Myc-Max transcriptional activity and subsequent downstream functions, to reduce viability in PCa cell lines, disrupt protein-DNA interactions and to induce apoptosis as their mechanism of action. Among compounds identified that effectively inhibit Myc-Max activity with low to mid-micromolar range potency and no or minimal generic cytotoxicity, VPC-70067, a close analog of the previously identified Myc inhibitor 10058-F4, served as proof-of-concept that our *in silico* drug discovery strategy performed as expected. Compound VPC-70063, of a chemically different scaffold, was the best performer in a panel of *in vitro* assays, and the forerunner for future hit-to-lead optimization efforts. These findings lay a foundation for developing more potent, specific and clinically optimized Myc-Max inhibitors that may serve as promising therapeutics, alone or in combination with current anti-cancer treatments, for treatment of specific phenotypes or heterogeneous tumors.

© 2018 Elsevier Masson SAS. All rights reserved.

1. Introduction

Myc is an essential regulator of growth in normal cells, but in many cancers this transcription factor is overactive to support high rates of growth needed for tumor proliferation and progression [1,2]. Myc drives tumorigenesis by transcriptional programming of a large number of target genes that promote cell growth, proliferation, metabolism and apoptosis, and block differentiation [3–7]. Myc is estimated to contribute to most if not all human cancers, including prostate, breast, colon, cervical cancers, small-cell lung carcinomas, neuroblastomas, osteosarcomas, glioblastomas, melanoma, and myeloid leukaemia, most of which are aggressive and respond poorly to the current therapies [1,8,9].

* Corresponding author. Vancouver Prostate Centre, 2660 Oak Street, Vancouver, British Columbia, V5H 3Z6, Canada.
  E-mail address: acherkasov@prostatecentre.com (A. Cherkasov).
  [1] Co-first authors.
  [2] Dr. Cherkasov's and Dr. Rennie's laboratories made equal contributions to this work.

In prostate cancer (PCa), the second leading cause of cancer-related death in men, Myc family members – L-Myc, c-Myc and N-Myc – are implicated in pathogenesis and progression across the full spectrum of PCa, from localized adenocarcinoma to the most advanced and treatment-resistant subtypes – castration-resistant (CRPC) and its neuroendocrine phenotype (NEPC). Amplifications of Myc family members are the most frequently observed genomic alterations associated with specific clinical stages and subtypes of PCa [10–16]. L-Myc is amplified in ~27% of localized PCa, in a mutually exclusive manner to c-Myc [11], whereas c-Myc is commonly amplified in all PCa stages and subtypes [17]. Notably, c-Myc overexpression antagonizes the transcriptional activity of the androgen receptor (AR), which is a driving force in PCa and constitutes the main drug target for advanced cases of disease [18]. Besides influencing clinically relevant AR target genes, c-Myc upregulation also affects critical splicing programs [19] and increases levels of AR-V7 - the constitutively active ligand-independent AR splice variant that promotes CRPC [20,21] and is also observed in NEPC [14]. Importantly, N-Myc amplifications induce the NEPC phenotype [14,15,22].

To elicit its oncogenic effects, Myc must form a heterodimer with its obligate partner Max, which together bind to the DNA and activate transcription of the target genes [23–26]. Although Myc could qualify as an ideal cancer target, applying conventional structure-based drug design approaches is inherently challenging in drugging Myc. Myc and Max are intrinsically disordered proteins (IDP) which exist as dynamic ensembles, with no effective pockets on their surfaces [27–29]. The disordered basic-helix-loop-helix-leucine zipper (bHLHLZ) domain of the Myc monomer forms DNA-binding functionalities only via association with the homologous bHLHLZ domain of Max [23,30]. Only upon such hetero-dimerization does the resulting Myc-Max complex adopt a stable helical configuration which can bind specific DNA recognition sequences 5′-CACGTG-3′, termed E-boxes, at enhancers and promoters of target genes, and thereby trigger the recruitment of chromatin-remodeling complexes and assembly of the transcriptional machinery to drive the transcriptional program [31,32]. Myc and Max oligomerize through their helix-loop-helix (HLH) and leucine zipper (LZ) regions and bind DNA mainly through highly positively charged basic (b) region and specific residues located in the HLH region [33,34].

Although Myc inactivation may have undesired effects on normal cells, experimental mouse models of KRAS-driven lung cancer carrying a conditionally inducible Omomyc construct – a Myc dominant negative, 93 residue bHLHZ protein fragment with 4 single-point mutations in the LZ region – established that periodic inhibition is effective at stopping cancer growth with mild and tolerable side effects, suggesting a viable therapeutic strategy [35,36].

Small molecule inhibition of Myc, a therapeutically compelling oncogenic transcription factor, has been a challenge for a long time. Current strategies that directly target Myc in cancer include inhibitors of Myc-Max protein-protein interactions, such as 10058-F4, 10074-G5, and JY-3-094 [37,38], or protein-DNA interactions, such as Mycro3 [39] and KJ-Pyr-9 [40], and inhibitors of Myc expression with G-quadruplex stabilizers, antisense oligonucleotides, and siRNA [41,42]. Indirect approaches have been reviewed elsewhere [41,43,44].

Compounds 10058-F4, 10074-A4, and 10074-G5 are among the first identified direct small molecules Myc inhibitors that bind with mid-micromolar range affinity at 3 independent sites on the disordered bHLHLZ domain of the Myc (c- and N-Myc) monomer (as validated by mutagenesis and NMR experiments) [37,45,46]. The efforts to identify them relied on functional screening of finite libraries unlikely to contain clinically-optimized structures.

Attempts to find more potent and selective analogs did not yet succeed given the inconsistent behavior of compounds in *in vitro* assays [47,48]. Moreover, these compounds lack proper antitumor activity *in vivo* due to rapid metabolism to inactive metabolites, resulting in low tumoral concentrations insufficient to inhibit Myc-Max dimerization [49,50]. Thus, the quest for discovering effective small molecule inhibitors of Myc is under way and several groups are actively pursuing this research.

2. Results and discussion

In this study, we identified a binding site on the DNA-binding domain (DBD) of the structurally ordered Myc-Max complex and employed a computer-aided drug discovery approach to identify small molecule binders that inhibit Myc-Max activity. A large-scale virtual screening protocol implementing structure-based methodologies was utilized to select a set of top-ranked compounds that were subsequently evaluated experimentally for their effect in inhibiting Myc-Max transcriptional activity, suppressing subsequent downstream functions, and reducing viability of various PCa cell lines. We further characterized the identified compounds for their ability to bind Myc-Max directly, to disrupt protein-DNA interactions, and to induce apoptosis. A number of prospective small molecules were identified that effectively inhibit Myc-Max activity with low to mid-micromolar range potency and with no or minimal generic cytotoxicity. Among these, compound 70067 highly similar in structure, potency and mechanism of action to 10058-F4, served as proof-of-concept to validate the *in silico* drug discovery strategy employed in this work. In addition, a distinct compound 70063 qualified as the best performer in a panel of *in vitro* assays, and has been selected for future optimization efforts based on observed structure activity relationships (SAR).

2.1. Identification of potentially druggable surface sites on the Myc-Max DNA-binding domain (DBD)

The published 1.9 Å crystal structure of c-Myc-Max heterodimer bound to its DNA-recognition sequence (PDB ID: 1NKP) [34] was selected for identification of plausible pockets where small molecules may bind and disrupt the c-Myc-Max DBD - E-box complex. Using the Site Finder module of the Molecular Operating environment (MOE) suite of programs [51], one potential binding site was predicted at the Myc-Max-DNA interface. MOE's Site Finder is a geometric method used to calculate possible active sites in a receptor from its 3D atomic coordinates and rank the sites according to their Propensity for Ligand Binding (PLB) score based on the amino acid composition of the pocket. As the highest PLB-ranked pocket, the predicted binding site was considered for targeting the Myc-Max DBD with small molecules. The pocket is located at the fork formed between the DNA-binding bHLH regions of c-Myc and Max, with which the dimer inserts itself into the DNA major groove (Fig. 1A). This site identified on the ordered dimer interface contains highly-conserved residues from both Myc and Max monomers and as such differs from the previously reported sites on the Myc disordered monomer. The pocket (Fig. 1B) is shaped by hydrophobic residues Leu917 and Phe921 from the c-Myc monomer and the equivalent residues Ile218 and Phe222 from the homologous Max monomer, and charged residues Lys939 from c-Myc, and Arg212, Arg215, Asp216, Lys219 and Arg239 from Max (see also Fig. 4B, section 2.6 for further details). The functional relevance of residues in the site was demonstrated by evidence from Max-Max [33] and Omomyc [52] homodimers crystallographic studies. It has been demonstrated that Arg215 in the basic region of Max makes both base-specific and contacts with the phosphate groups of the DNA backbone, dictates the identity of the central 5′-CG-3′
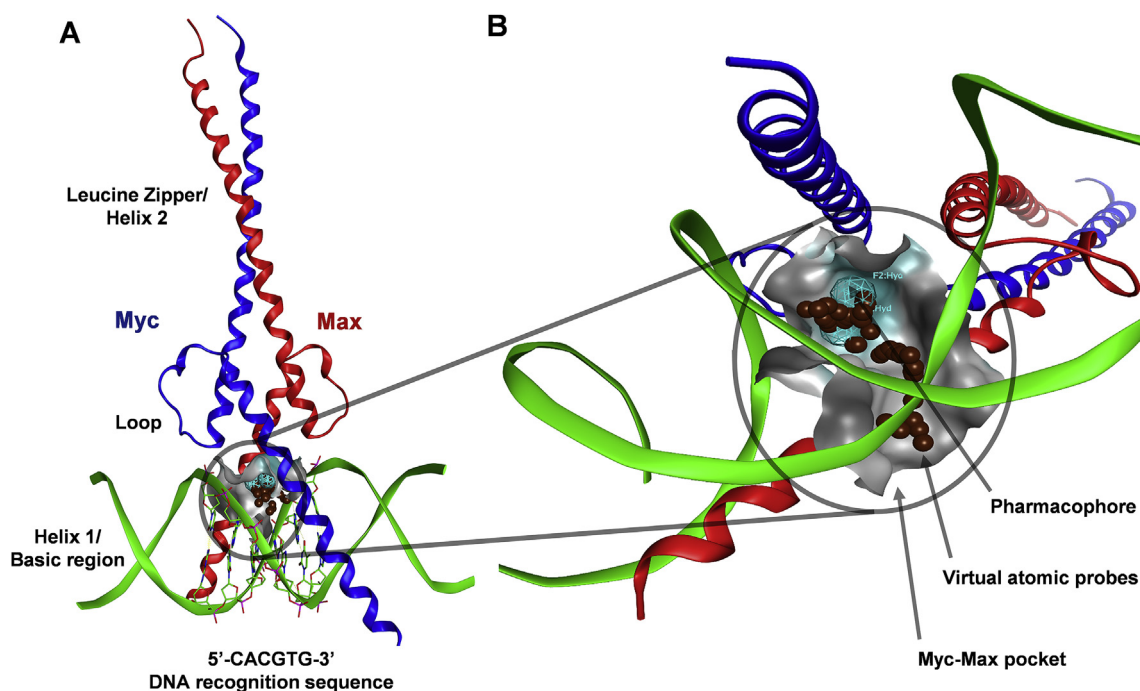
Fig. 1. (A) *In silico* model of the basic/helix-loop-helix/leucine zipper (bHLHZ) domain of Myc-Max bound to the 5′-CACGTG-3′ DNA recognition sequence. The model was constructed based on the 1.9 Å crystal structure of Myc-Max heterodimer in its bound form to the canonical E-box sequence (PDB ID: 1NKP). Myc (blue), Max (red) and the DNA backbone (green) are represented as ribbons. The DNA bases forming the E-box recognition sequence are represented as sticks. The Myc-Max predicted binding site at the DNA interface (side view) is represented as a grey solid surface and emphasized with a black circle; (B) Magnified view of the Myc-Max predicted binding site (bottom view of the structure of the complex in panel A which is rotated 90° on the horizontal axis). The site was identified by probing the surface with virtual atoms (brown spheres within the pocket). The residues shaping the pocket are described in the text and further detailed in Fig. 4B. The pharmacophore utilized for subsequent virtual screening and filtering of potential binders is shown as cyan meshed spheres (see text for details). Inhibitors targeting the predicted site are expected to block Myc-Max binding to DNA.

dinucleotide of the canonical E-box sequence, and appears to be essential for DNA binding. Similarly, Arg239 of Max makes side-chain and backbone amide contacts with phosphate groups of DNA backbone, tethers Helix-2 to DNA, and stabilizes the interactions between Helix-1 and Helix-2 by packing against Phe222 conserved hydrophobic residue in Helix-1. Arg239 is important for both dimerization and DNA binding. Lys939 of Myc, the counterpart of Arg239 of Max, makes specific contacts with phosphate groups of DNA backbone [33]. A recently reported comparison of the protein-DNA interface of Omomyc to that of the Myc-Max DNA complex [52] demonstrated that both complexes bind to the DNA major groove by forming a scissor-like structure at the E-box, and that the basic region of both complexes assumes the same phosphate-backbone and base-specific contacts to DNA, an example of which is Arg914 of Myc (Arg20 of Omomyc), the equivalent of Arg215 of Max. Thus, the positively charged residues lining up the identified site may provide hydrogen bonding and/or salt bridges propensity for potential binders to disrupt the above-mentioned DNA base and phosphate contacts while the hydrophobic core of the site may substantially anchor the binders via hydrophobic interactions. Inhibitors targeting the predicted site are expected to block Myc-Max binding to DNA.

2.2. In silico identification of hit compounds targeting the Myc-Max DBD site

The drug-like subset of the ZINC12 molecular database [53,54], containing more than 6 million purchasable chemicals, was further reduced to 4.7 million compounds by filtering by physicochemical properties such as charge, number of rings and rotatable bonds. The resulting set of 4.7 million structures was virtually screened against the identified pocket on the Myc-Max dimer DBD. Glide (Maestro
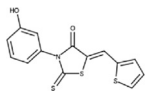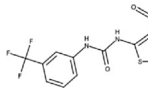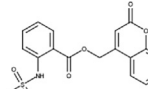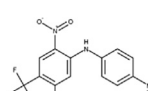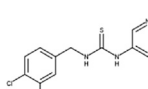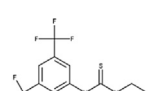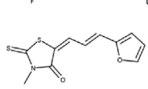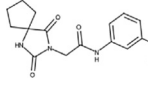
9.3 suite, Schrödinger LLC) software [55–57] was employed as the primary structure-based docking technique (with the standard precision mode). The generated docking poses were then filtered by the Glide docking score (binding energy score used to rank docking poses and distinguish strong binders in their optimal placement in the respective pocket from compounds that bind weakly) using a −5.5 kcal/mol cutoff. The top ranked 12503 remaining compounds were further filtered by structure-based pharmacophore screening using MOE's tools. A pharmacophore model of two essential hydrophobic features (1.5 Å diameter each) of the binding site (formed primarily by Leu917, Ile218, Phe921 and Phe222) was built and used to search for matching hits in the database of top ranked Glide poses (Figs. 1B and 4A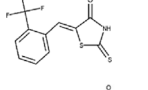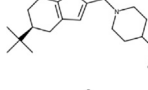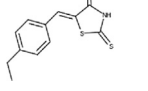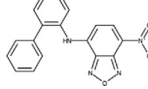). 1019 pharmacophore-matching hits were then selected for visual inspection. 116 compounds having a good balance of Glide docking score and ligand efficiency (the ratio of binding affinity over the number of heavy atoms) made additional side-chain or backbone hydrogen bonds with the charged residues in the site. 69 chemicals were selected for purchase, in particular those predicted to form hydrogen bonds with the backbone carbonyl oxygen of Arg215. The purchased compounds were then subjected to rapid evaluation using a primary screening transcriptional assay (see below). From the primary cell-based screening 10 hits were identified (Table 1) showing better than 50% inhibition of Myc-Max transcriptional activity. Hits with more than 70% inhibition were further investigated for effect on the downstream pathway using UBE2C reporter assay.

2.3. Effects of hit compounds on Myc-Max transcriptional activity

Compounds were subjected to experimental evaluation using the commercially available transcriptional assay Cignal c-Myc luciferase reporter assay in LNCaP cells. Compounds 10058-F4 and

Table 1
Docking scores and activities of hit compounds that bind the ordered Myc-Max DBD at the identified site.

Compound ID	Structure	Glide docking score (kcal/mol)	Myc-Max transcriptional activity %inhibition (25 μM)	Myc-Max/UBE2C downstream pathway %inhibition (25 μM)
VPC-70005		−5.53	65	n/a
VPC-70021		−5.63	95	73
VPC-70027		−5.69	53	n/a
VPC-70033		−5.77	81	51
VPC-70053		−5.66	73	50
VPC-70063		−5.51	106	94
VPC-70064		−5.59	78	64
VPC-70066		−5.77	65	n/a
VPC-70067		−5.67	98	71
VPC-70068		−5.68	73	58
10058-F4		n/a	91	70
10074-G5		n/a	88	n/a

10074-G5, known Myc inhibitors from the literature, were used as positive controls. A transiently transfected Myc-driven luciferase reporter allowed the monitoring of Myc-regulated signal in LNCaP upon treatment with the *in silico* identified compounds. From a larger number of hits, 10 compounds caused more than 50% reduction of the Myc-driven luciferase levels at 25 μM (see Table 1). A thorough dose response analysis was performed using LNCaP cells to evaluate the potency of hit compounds. The compounds inhibit Myc-Max transcriptional activity with low to mid-micromolar potency, with the following IC_{50} values (half-maximal inhibitory concentration with 95% Confidence Intervals) established as: 22.7 μM [16.6–31.2 μM] for VPC-70067 comparable to

that of the control compound 10058-F4 (28.9 μM; [19.7–42.5 μM]), and 8.9 μM [6.6–11.8 μM] for VPC-70063 (Fig. 2A).

2.3.1. Effects of hit compounds on Myc-Max downstream-regulated pathways

Myc inhibition was recently reported to reduce levels of the constitutively active androgen receptor splice variant AR-V7 in 22rv1 cells [20]. AR-V7 has been shown to specifically regulate the expression level of the Ubiquitin Conjugating Enzyme E2C (UBE2C) in androgen-deprived 22rv1, through the UBE2C promoter [21]. Hence, a complementary transcriptional screening assay was developed *in house* to monitor the expression levels of the AR-V7
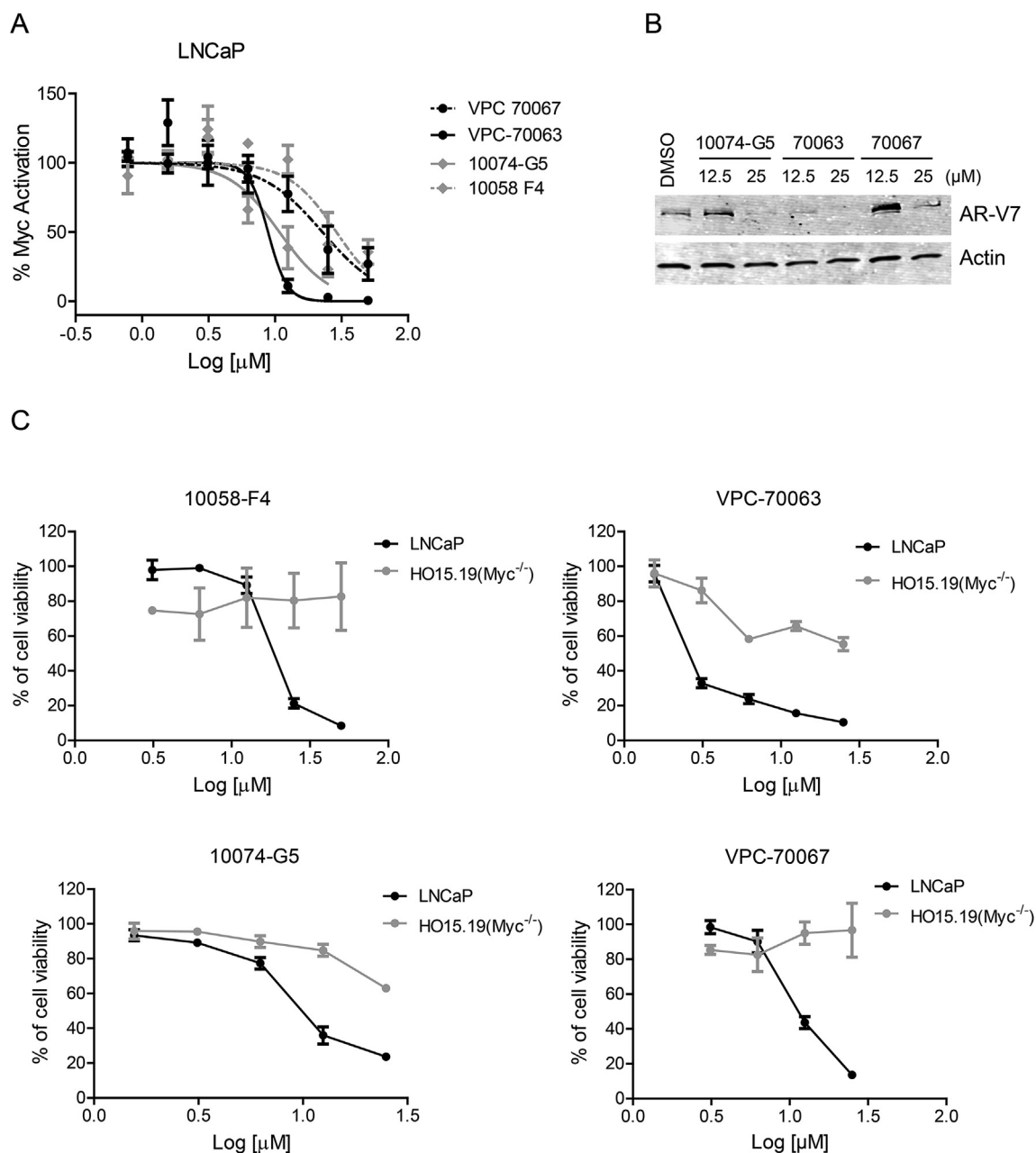
Fig. 2. (A) Dose response effect of selected hits in LNCaP PCa cells on the transcriptional activity of c-Myc by using a c-Myc mediated luciferase reporter. Literature inhibitors 10058-F4 and 10074-G5 were used as positive controls. Data are presented as mean ± SEM of triplicates and expressed as a percentage of luciferase activity relative to DMSO control. (B) Inhibition of Myc-Max reduces the levels of AR variant 7 in 22rv1 cells. (C) The effect of VPC-70063 and VPC-70067 in comparison with 10058-F4 and 10074-G5 on cell viability of Myc positive (LNCaP) and Myc negative (HO15.19) cell lines. The percent of cell viability is plotted in dose dependent manner. Data points represent the mean ± 95%CI (confidence interval) of triplicates and expressed as percent of cell viability relative to DMSO control.

isoform in 22rv1 cells by using a plasmid containing a UBE2C promoter linked to a luciferase reporter. The dose-dependent reduction of luciferase levels by the identified hits indicates a Myc-related reduction of AR-V7 level in the cells (see Table 1). Compound VPC-70063 showed the highest reduction of UBE2C promotor activity suggesting the reduction of V7 levels in 22rv1. The AR-V7 reduction with the hits was confirmed by Western blot (Fig. 2B).

2.4. Effects of hit compounds on cell viability

The effect of hit compounds on Myc-driven cell proliferation was evaluated by measuring the cell viability of LNCaP cells after treatment with increasing concentrations of compounds. Again, VPC-70063 showed the best inhibition of LNCaP cell proliferation (IC50 = 2.5 μM; [95%CI: 2.1–2.8 μM]. To rule out that this inhibition was due to non-specific cytotoxicity of VPC-70063 we therefore treated the c-Myc knockout HO15.19 cell line (Fig. 2C) with this compound. The proliferation of the HO15.19 cell line was slightly affected by VPC-70063, up to a maximum of 40% inhibition at 25 μM. However, at a VPC-70063 concentration of 3 μM where 70% of LNCaP cells are inhibited there was no significant effect on the c-Myc knockout cells. VPC-70067, 10058-F4 and 10074-G5 have IC50 of 11.1 μM [95%CI: 10.6–11.4 μM], 18.31 μM [95%CI: 17.7–18.8 μM] and 8.7 μM [95%CI: 8.3–9.1 μM], respectively (Fig. 2C).

2.5. Mechanism of action of hit compounds

2.5.1. Apoptosis

Myc inhibition induces cell death by cell cycle arrest and apoptosis [58]. Cleavage of PARP-1 by caspases is considered a hallmark of apoptosis and so we measured the ability of compounds to induce PARP cleavage after treatment. As predicted, VPC-70063 and VPC-70067 were inducing PARP cleavage suggesting that the effect of these two compounds were through apoptotic pathways (Fig. 3A).

2.5.2. Direct binding and disruption of protein-DNA interaction

To study the direct effect of our hit compounds VPC-70063 and VPC-70067 on the interaction between Myc-Max heterodimer and the DNA, we used Bio-Layer Interferometry (BLI, ForteBio). This technique is a label-free technology allowing the measurement of direct interactions between two partners, one immobilized on a sensor and the other one present in a solution. We applied this technology to study the disruption of the interaction between a biotinylated E-box oligo immobilized on a streptavidin biosensor and a purified Myc-Max complex in presence of our compounds. Therefore, histidine-tagged Max (residues 23—102) and GST tagged Myc (residues 368—454) were overexpressed and co-purified. The fraction containing equal amount of Myc and Max was collected and used for the binding assay (Fig. 3B). The presence of both proteins was validated by Western blot using a specific antibody of each protein. Using BLI, we were able to show that Myc-Max heterodimer was prevented from interacting with the immobilized DNA in presence of both VPC-70063 and VPC-70067 similarly to the control 10074-G5 (Fig. 3C). Additionally, we tested the ability of our best compound VPC-70063 to disrupt the interaction of Myc-Max with DNA in a dose dependent manner. At a concentration below 100 μM, we did not see any significant effect on the complex dissociation. But at higher concentration we noticed a dose response decrease of the Myc-Max binding to DNA showing that VPC-70063 was able to disrupt the complex formation (Fig. 3D).

2.5.3. Effect of inhibitors on Myc-Max interaction using mammalian 2-hybrid assay

We next studied the effect of inhibitors of Myc-Max interaction by using a mammalian two hybrid assay. Full lengths Myc and Max were cloned in pBIND and pACT plasmids (CheckMate, Promega), respectively. Luciferase levels corresponding to Myc-Max interactions were measured and normalized to a control provided by the commercial kit to discard non-specific effect due to toxicity or direct luciferase inhibition. VPC-70063 showed a dose response inhibition of the interaction between the two proteins (Fig. 3E). Unexpectedly, 10074-G5 did not show any effect on Myc-Max interaction in this assay. As VPC-70063 is more potent than 10074-G5 in most of the other assays, higher concentrations of the latter may be needed to see an inhibition of the interaction.

2.6. In silico binding mode of VPC-70063

As described above, compound VPC-70063 was the best performer in all the cell-based and cell-free assays designed for this study. The predicted binding pose of VPC-70063 (1-benzyl-3-(3,5-bis(trifluoromethyl)phenyl)thiourea), obtained using computational modeling methods, is shown in Fig. 4. The chemical structure of VPC-70063 is composed of a benzyl ring at one end, a thiourea linker and a highly hydrophobic 3,5-bis(trifluoromethyl)phenyl moiety at the other end. Within the binding pocket of the Myc-Max DBD domain, VPC-70063 is predicted to form 2 hydrogen bonds between the 2 thiourea amine hydrogens and the backbone carbonyl of Arg215 (Fig. 4B, magenta dashed lines), as well as a large

number of strong hydrophobic interactions (Fig. 4B, green dashed lines) formed by the 3,5-bis(trifluoromethyl)phenyl moiety with the hydrophobic core of the pocket, including aliphatic and aromatic side-chains of Leu917, Phe921, and Lys939 of Myc, and Ile218, Phe222, and Arg215 of Max, and those formed by the benzyl ring with aliphatic side chains of Arg215 and Arg212 of Max. Noteworthy, as shown in Fig. 4A, the 3,5-bis(trifluoromethyl)phenyl group of VPC-70063 is matching the hydrophobic features of the constructed pharmacophore, it is deeply buried in the hydrophobic core of the Myc-Max DBD pocket being stabilized via hydrophobic interactions. Furthermore, in the binding pose, the benzyl ring of VPC-70063 is predicted to overlap significantly with the DNA backbone. Therefore, it was expected that VPC-70063, in as much as other hits having similar interactions, would overcome the binding of DNA to the Myc-Max DBD site. It is not surprising then, that VPC-70063 blocks the binding of Myc-Max to DNA as determined by BLI measurements. Further experiments are required to unequivocally prove the binding mode and direct disruption of protein-DNA interactions with our current hits and future derivatives.

3. Discussion and future perspectives. Hit-to-lead optimization

Findings reported in this study prompted us to leverage the full power of our *in silico* drug discovery platform that proved successful in targeting unconventional sites on protein surfaces and in yielding promising preclinical drug candidates for previously uncharted targets [59—67]. Consequently, we have initiated ligand-based similarity searches followed by molecular docking and consensus scoring computations to identify analogs of the initial hit compounds (Fig. 5A). Briefly, three-dimensional similarity searches are conducted utilizing the ROCS program from OpenEye [68,69] against a large ensemble of conformers consisting of at most 200 conformers for each of the approximately 9 million entries of the drug-like purchasable chemical space of the ZINC15 database [70]. Conformers are generated using Omega2 of OpenEye [71]. Current hits are used as query molecules. ROCS is a fast shape-based superposition method, which uses a combination of global three-dimensional shape overlay and color-based chemical complementarity in terms of hydrogen-bond donors, hydrogen-bond acceptors, hydrophobes, anions, cations and rings, to compare the query to a large collection of molecules and rank the matching hitlist according to the TanimotoCombo score, a rigorous measure of shape and color overlap. Molecular docking, using 3 docking programs differing in their underlying scoring functions and sampling algorithms: Glide [55,56], ICM [72] and Hybrid [73,74], is employed to position analogs into the Myc-Max DBD. Consensus voting and filtering using various thresholds is subsequently performed. The consensus is built based on top-ranking docking scores (the more negative the stronger the binding affinity; e.g. Glide score ≤ -5.5 kcal/mol) and calculation, using MOE scripts [75,76], of two indicators: root mean square deviation (RMSD), an atom-based metric reflecting the deviation in atomic coordinates between poses obtained from the three docking programs, and predicted pKi, a good indicator of potency. The filtering thresholds used are: RMSD ≤ 3 Å (an RMSD of 0 indicates perfect superposition; the higher the RMSD the greater the deviation), and pKi ≥ 5 (the larger more potent theoretically). All high-confidence analogs are subsequently subjected to full experimental profiling. Quantitative (QSAR) models based on our *in house* developed 3D and 4D inductive descriptors [77,78] are currently customized for Myc-Max target to serve as an additional scoring function for accurate activity prediction of analogs and future derivative series.

In the longer term and as per our usual practices [79], the target affinity and drug-like profile of the most promising analogs will be
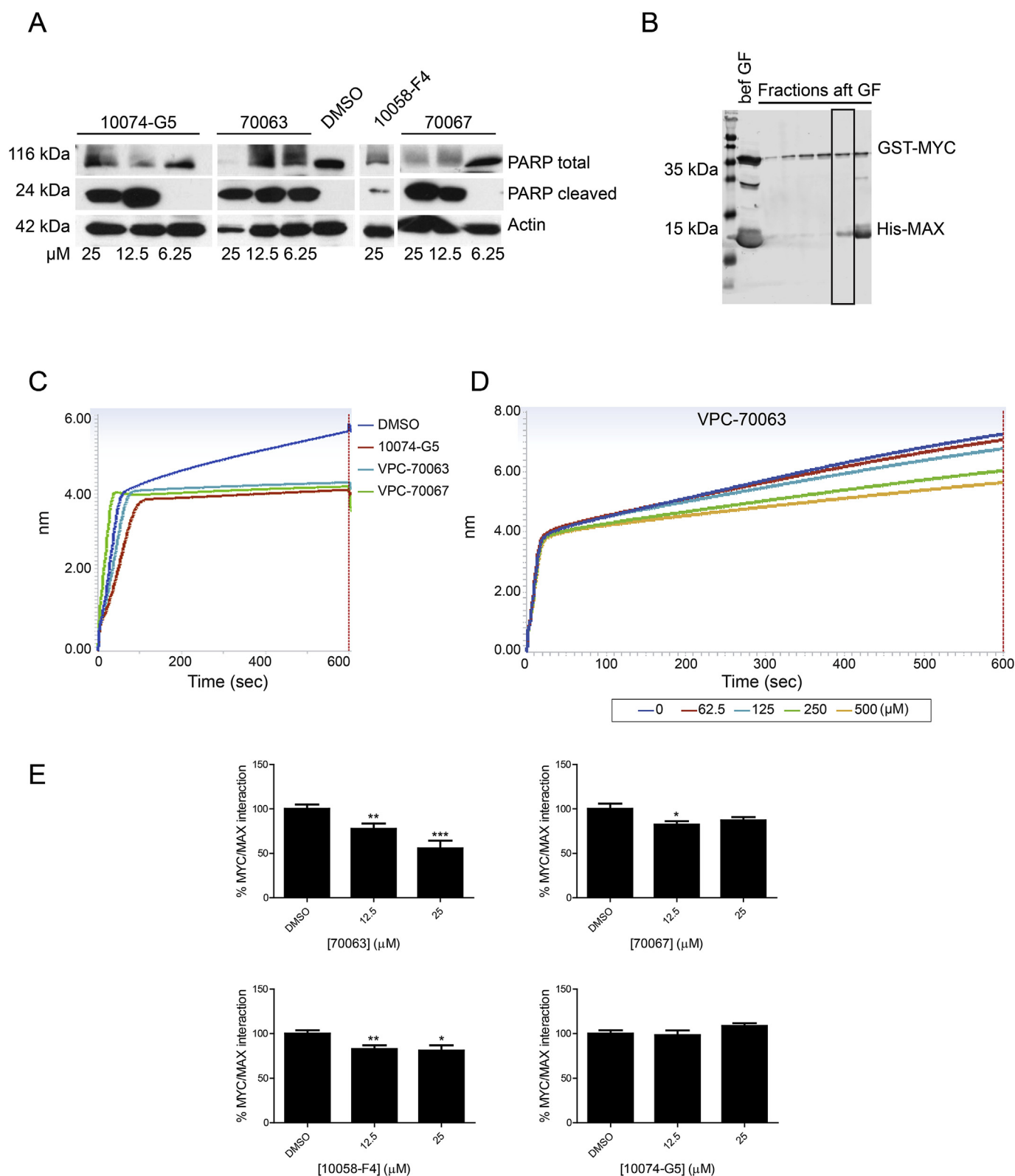
Fig. 3. (A) Inhibition of Myc with VPC-70067 and VPC-70063 resulted in apoptosis of LNCaP cells as indicated by cleavage of PARP in Western blot. (B) Purification of GST-Myc and His-Max using size exclusion chromatography. The fraction highlighted with a black rectangle on the Western blot corresponds to the fraction used for the binding assay. (C) Inhibition of Myc-Max interaction with the biotinylated E-box quantified by bilayer interferometry (BLI) in presence of 500 μM of the studied compounds. (D) Dose response inhibition of Myc-Max binding to DNA in presence of best compound VPC-70063. (E) Mammalian 2-hybrid assay showing the effect of inhibitors on the interaction between Myc and Max. Data points represent the mean ± SEM of at least three independent experiments. P < 0.05 (*), P < 0.01 (**) and P < 0.001 (***) were considered statistically significant compared with vehicle control (two-tailed t-test).
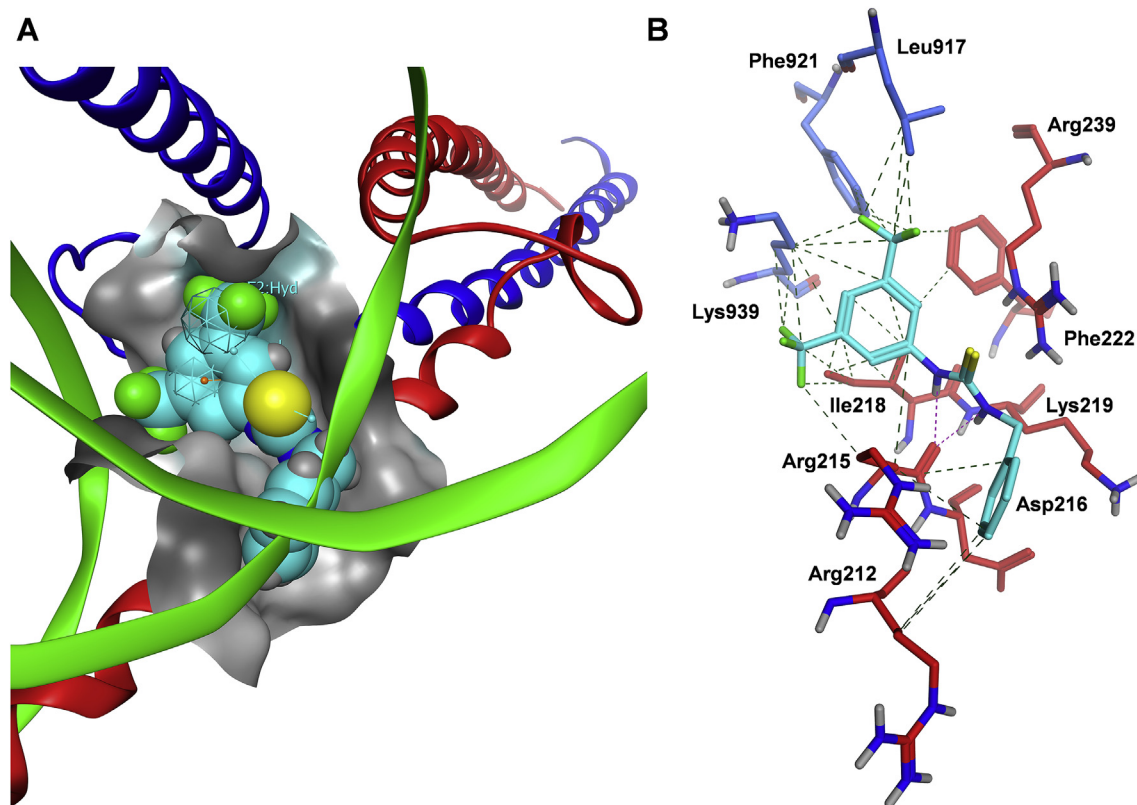
Fig. 4. (A) Predicted binding pose of VPC-70063 in space-filling representation within the Myc-Max DBD pocket (cyan = carbon, blue = nitrogen, green = fluorine, yellow = sulfur). Myc, Max, the DNA backbone and the pocket are colored using the same scheme as in Fig. 1. The chemical structure of VPC-70063 (1-benzyl-3-(3,5-bis(trifluoromethyl)phenyl) thiourea) is discussed in the text. The 3,5-bis(trifluoromethyl)phenyl moiety of VPC-70063 is deeply buried in the hydrophobic core of the pocket. The benzyl ring of VPC-70063 significantly overlaps with the DNA backbone. VPC-70063 is expected to compete with DNA for binding to the Myc-Max DBD pocket; (B) Pocket residues predicted to interact with VPC-70063 at the Myc-Max DNA interface. Hydrogen bonds formed by the thiourea moiety of VPC-70063 are indicated with magenta dashed lines. Hydrophobic stabilizing interactions formed by the benzyl ring as well as the phenyl ring and the trifluoromethyl groups are represented with green dashed lines. Protein residue numbering follows that from the crystal structure of Myc-Max dimer (PDB ID: 1NKP; chains A, B).

optimized based on observed structure activity relationships (SAR) in iterative rounds of *in silico* modeling, medicinal chemistry and biological validation, until a lead is found (Fig. 5B). In this process, for more elaborate and accurate scoring, computationally-demanding classical molecular dynamics (MD) and free energy perturbation MD simulations [80–85] will be executed on GPU-accelerated clusters. Moreover, the drug-like profile of promising derivatives will be improved by eliminating toxic moieties and metabolically labile centers as predicted by Simulations Plus ADMET Predictor software [86]. This approach will allow us to achieve highly potent binding while maintaining the ligand properties required for safety and biological efficacy.

4. Conclusions

In the absence of clinically approved anti-Myc drugs, targeting the Myc-Max complex represents a critical step towards creating new therapeutics for lethal CRPC and NEPC. In this study, we identified a possible druggable site on the DNA-binding domain (DBD) of the structurally ordered Myc-Max complex and employed a computer-aided rational drug discovery approach to identify small molecules that inhibit Myc-Max functionality. A large-scale virtual screening protocol was utilized to select a set of top-ranked compounds that were subsequently characterized experimentally. A number of compounds were identified that inhibit Myc-Max activity with low to mid-micromolar potency and with no or minimal cytotoxicity, including VPC-70067, a compound

highly similar in structure, potency and mechanism of action to 10058-F4. In addition, a novel compound VPC-70063 with a chemically different scaffold was identified as the best performer in a panel of *in vitro* assays as it inhibits Myc-Max transcriptional activity (IC$_{50}$ = 8.9 μM; [95% CI: 6.6–11.8 μM]), Myc-Max downstream functions, levels of the AR-V7 splice variant in CRPC cells, and cell growth in various PCa cell lines. In addition, VPC-70063 induces apoptosis as expected with a Myc inhibitor. Its specificity was further illustrated by the observed inhibitory effect on the Myc-Max association with DNA and by the cell viability experiment with Myc-negative cell line HO15.19. It should be noted, however, that in the latter system some cytotoxicity has been detected at higher concentrations of VPC-70063. Even though the extent of inhibition of Myc-negative cells was much less profound than that for Myc-positive ones (7% versus 50% at 2.5 μM administration), the observed general cytotoxicity is a concern and will be addressed in our future optimization efforts for VPC-70063 series of Myc-Max inhibitors. On the other hand, it should also be mentioned that the positive control we have used − a compound 10074-G5 has also demonstrated 37% suppression of HO15.19 at 25 μM dosage. The most recently reported small molecule Myc-Max inhibitor MYCMI-6 has also exhibited about 15% inhibition of HO15.19 at 10 μM [87]. Thus, it is not impossible to speculate that those inhibitors could affect other Max containing complexes in HO15.19 cell line and/or that the corresponding prototypical small molecule Myc-Max inhibitors all require further optimization and reduction of Myc-independent cytotoxicity. As before, our integrative approach to
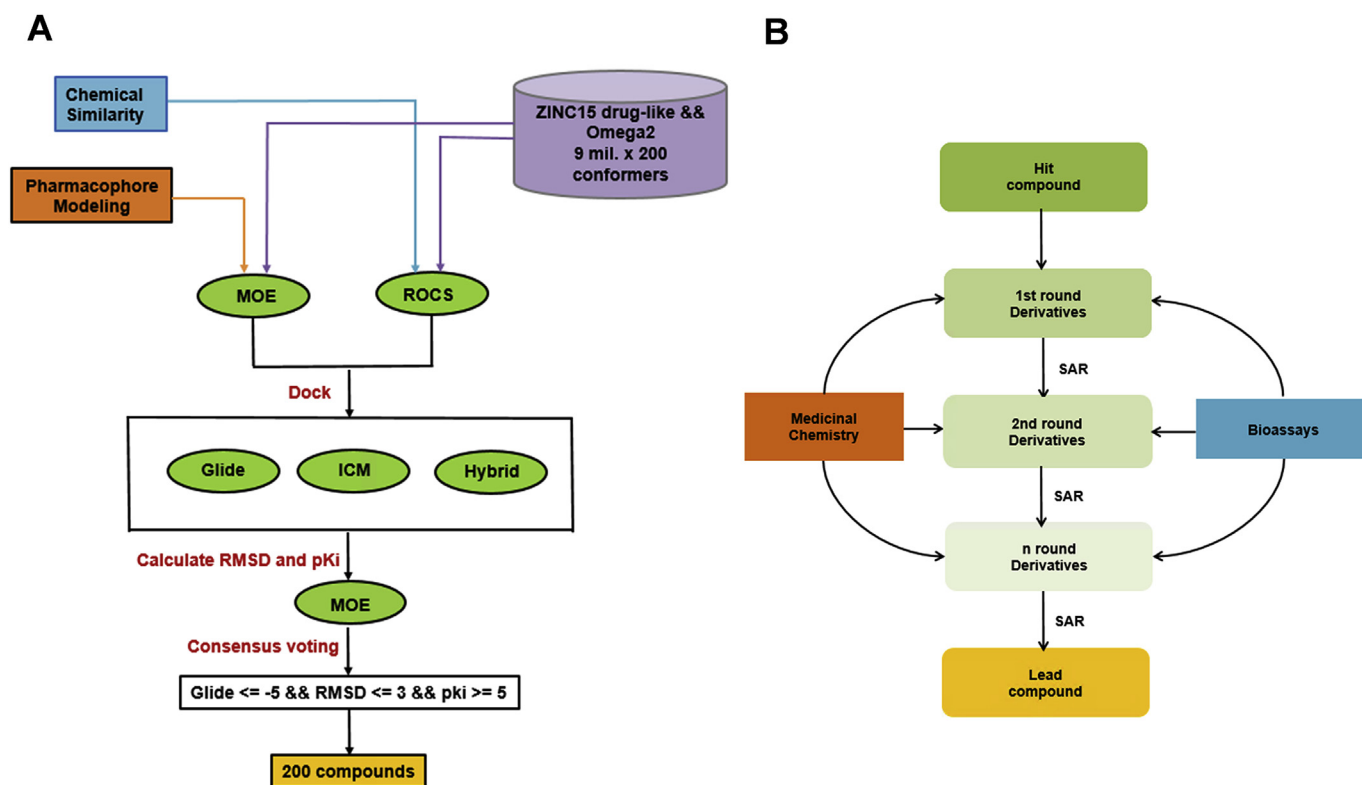
A

B

Fig. 5. (A) Virtual screening protocol implementing structure-based and ligand-based methodologies and consensus scoring for ranking and selection of analogs with potentially enhanced potency starting from initial hits. Using consensus voting based on docking scores, RMSD deviation between poses generated by various docking programs, calculated pKi and filtering using various thresholds, a small number of compounds can be selected for experimental testing from the millions at the start. (B) Lead optimization protocol consisting of iterative rounds of *in silico* modeling, medicinal chemistry and biological validation based on observed structure-activity relationships (SAR). Accurate prediction of relative binding free energy between hit and morphed derivatives obtained from free energy perturbation molecular dynamics simulations, as well as control of the ADMET profile of *in silico* constructed derivatives are state-of-the-art methods used for prioritization of derivatives for next iteration of SAR until a lead is found.

drug discovery proved successful insofar in discovering novel Myc-Max inhibitors as promising far-reaching therapeutics for advanced prostate and other cancers.

5. Materials and methods

5.1. Virtual screening of potential Myc-Max DBD inhibitors

The published 1.9 Å crystal structure of c-Myc-Max heterodimer bound to its DNA-recognition sequence (PDB ID:1NKP [34], chains A, B; waters and DNA excluded) was subjected to the Site Finder algorithm implemented in MOE [51]. Site Finder is a geometric method which uses alpha spheres (virtual atoms) to probe a protein surface for suitable small molecule binding pockets. Briefly, Site Finder first identifies regions of tight atomic packing, filters out highly solvent exposed sites, calculates alpha spheres on sites and classifies them as either hydrophobic or hydrophilic depending on whether the virtual atom is in a good hydrogen bonding spot in the receptor, and then produces a collection of sites based on pruning (alpha spheres corresponding to inaccessible regions or exposed to solvent are eliminated) and clustering (by number and chemical type) of alpha spheres. The sites are then ranked according to their Propensity for Ligand Binding (PLB) score. The top PDB-ranked pocket was used for subsequent *in silico* screening. Virtual screening of the ZINC12 database [53,54] was performed using structure-based methods including molecular docking algorithms and pharmacophore screening. The Glide program [55,56], part of Maestro 9.3 suite, Schrödinger LLC [57], was used as the starting point to perform rigid docking of 4.7 million drug-like chemicals.

Following Maestro's standard protein preparation protocol [88,89], applied to the Myc-Max X-ray structure, a docking grid was defined as a 20 Å box centered on the residues of predicted Myc-Max DBD binding site for Glide sampling and scoring of screening compounds. Prior to docking, each chemical was washed and energy-minimized under the MMFF94× force field and Born solvation as per ligand preparation protocol implemented in MOE [51]. Docking was conducted using Glide standard precision mode with all other settings set to default. The generated docking poses were ranked by the Glide score, an interaction energy score that includes hydrogen bonding and hydrophobic interactions contributions. Potentially weak binders (Glide score > −5.5 kcal/mol) were discarded. The remaining top-ranked 12503 remaining compounds were further filtered by structure-based pharmacophore screening using MOE's tools [51]. A pharmacophore model of two essential hydrophobic features (1.5 Å diameter each) of the binding site (formed primarily by Leu917, Ile218, Phe921 and Phe222) was built and used to search for matching hits in the database of top ranked Glide poses. 1019 pharmacophore-matching hits were then selected for manual inspection using the 3D visual environment in MOE. 69 compounds having a good balance of Glide docking score and ligand efficiency and making favorable interactions with the surrounding side chains in the pocket were purchased for subsequent experimental testing.

5.2. Cell culture and reagents

LNCaP and PC3 cells were purchased from the ATCC and grown in RPMI 1640 supplemented with 10% fetal bovine serum (FBS). HO15.19 cells were a generous gift from John Sidivy at Brown

University and were cultured in Dulbecco's modified Eagle's medium DMEM (ATCC 30−2002) supplemented with 10% FBS. 10058-F4 and 10074-G5 were obtained from Sigma. The UBE2C reporter plasmid was purchased from GeneCopoeia (product ID #HPRM16429). The Biolux Gaussia luciferase assay kit was purchased from New England Biolab (#E3300L). PrestoBlue cell viability reagent was purchased from Invitrogen #A-13262.

5.3. Transfection and reporter assays

Cell transfection was performed using TransIT-2020 transfection reagents according to the manufacturer's instructions (Mirus). LNCaP cells were plated at 10000 cells per well and treated for 1 day with the indicated concentration of compound. Myc reporter activity was measured using the Cignal Myc Reporter Assay Kit from Qiagen (#336841) according to the manufacturer's instructions. For the UBE2C reporter assay, 22rv1 cells were plated at 10000 cells per well in 96-well plates in RPMI media supplemented with 5% charcoal-stripped serum (CSS) and treated for 1 day with 1 µM, 10 µM and 25 µM of compound.

5.4. Cell viability assays

LNCaP were plated at 5000 cells per well in RPMI 1640 containing 5% CSS in a 96-well plate, treated with test compounds (0−25 µM) for 96 h. Cell density was measured using the PrestoBlue assay according to the manufacturer's protocol. The percentage of cell survival was normalized to the cell density of control wells treated by vehicle. Viability of Myc-negative HO15.19 cells was done similarly but in DMEM supplemented with 5% CSS.

5.5. c-Myc-Max purification

Histidine tagged Max (residues 23−102) and GST tagged Myc (residues 368−454) were overexpressed in *E. coli* BL21-DE3 cells. Cells were co-lyzed in lysis buffer (20 mM Tris pH 8, 500 mM NaCl, 5% glycerol, 10 mM imidazole, 8 mM BME, 2.1 mM PMSF). After sonication and centrifugation, the complex was first purified by using a Ni-NTA affinity resin. After overnight dialysis to remove the imidazole, the protein sample was applied to a size exclusion chromatography equilibrated with (20 mM Tris pH 8, 150 mM NaCl, 5% glycerol, 0.2 mM TCEP). Fractions containing equal amount of Myc and Max on SDS PAGE were collected and used for the binding assay. The presence of both proteins was validated by Western blot using a specific antibody of each protein (Max (h2) Sc-8011 and c-Myc (9E10) Sc-40, Santa Cruz Biotechnology).

5.6. Biolayer interferometry assay

The direct interaction between biotinylated E-box oligo (TGAAGCAGACCACGTGGTCGTCTTCA) immobilized on a streptavidin biosensor and a purified Myc-Max complex (0.05 mg/ml) was quantified by BLI using OctetRED (ForteBio). The DNA was first bound to the super-streptavidin sensors over 1000 s at 25 °C. The sensors were next moved into wells containing the reaction buffer (20 mM Tris pH 8, 150 mM NaCl, 5% glycerol, 0.2 mM TCEP, 5% dimethylsulfoxide) for measuring the baseline and next into the Myc-Max complex alone or in presence of the tested inhibitors to study the association of the complex to the DNA.

5.7. Western blotting

After 48 h of treatment with compounds, LNCaP cells were lysed, and protein sample preparation followed by Western blotting were performed. Blots were incubated with primary antibodies against c-Myc, PARP (Sigma 084M4766V), PARP cleaved-Asp214 (Sigma SAB4500487) and β-Actin (Sigma A2066) overnight at 4 °C, followed by appropriate peroxidase-conjugated secondary antibodies. β-actin served as an internal control. Visualization of the immunocomplexes was done by an enhanced chemiluminescence detection system (Millipore) followed by exposure to X-ray films.

5.8. Mammalian two-hybrid assay

Full lengths Myc and Max were cloned in pBIND and pACT plasmids (CheckMate, Promega), respectively. PC3 cells in RPMI 1640 supplemented with 5% FBS were seeded in 96-well plates at 5000 cells/well. After 24 h, cells were transfected with 15 ng of pACT-Max, 19.5 ng of pBIND-Myc, and 13.6 ng of the reporter plasmid PG5-luciferase. After 24 h, cells were treated with various concentrations of the tested inhibitors. Cells were lysed the next day, and the luminescence signal was measured after adding 50 µL of luciferase assay reagent (Promega). Each measurement was done in 4 replicates with biological replicates of 3. Luciferase levels corresponding to Myc-Max interactions were measured and normalized to a control provided by the commercial kit to discard non-specific effect due to toxicity or direct luciferase inhibition.

Conflicts of interest

The authors declare no conflicts of interest.

Acknowledgements

References

[1] C.V. Dang, MYC on the path to cancer, Cell 149 (2012) 22−35.
[2] C.V. Dang, MYC, metabolism, cell growth, and tumorigenesis, Cold Spring Harbor perspectives in medicine 3 (2013).
[3] C.V. Dang, L.M. Resar, E. Emison, S. Kim, Q. Li, J.E. Prescott, D. Wonsey, K. Zeller, Function of the c-Myc oncogenic transcription factor, Exp. Cell Res. 253 (1999) 63−77.
[4] R. Ponzielli, S. Katz, D. Barsyte-Lovejoy, L.Z. Penn, Cancer therapeutics: targeting the dark side of Myc, Eur. J. Canc. 41 (2005) 2485−2501.
[5] M. Huang, W.A. Weiss, Neuroblastoma and MYCN, Cold Spring Harbor perspectives in medicine 3 (2013) a014415.
[6] Z.E. Stine, Z.E. Walton, B.J. Altman, A.L. Hsieh, C.V. Dang, MYC, metabolism, and cancer, Canc. Discov. 5 (2015) 1024−1039.
[7] S.B. McMahon, MYC and the control of apoptosis, Cold Spring Harbor perspectives in medicine 4 (2014) a014407.
[8] M. Gabay, Y. Li, D.W. Felsher, MYC activation is a hallmark of cancer initiation and maintenance, Cold Spring Harbor perspectives in medicine (2014) 4.
[9] D. Horiuchi, B. Anderton, A. Goga, Taking on Challenging Targets: Making MYC Druggable, American Society of Clinical Oncology Educational Book, American Society of Clinical Oncology, 2014, pp. e497−502. Meeting.
[10] C.M. Koh, C.J. Bieberich, C.V. Dang, W.G. Nelson, S. Yegnasubramanian, A.M. De Marzo, MYC and prostate cancer, Genes & cancer 1 (2010) 617−628.
[11] P.C. Boutros, M. Fraser, N.J. Harding, R. de Borja, D. Trudel, E. Lalonde, A. Meng, P.H. Hennings-Yeomans, A. McPherson, V.Y. Sabelnykova, A. Zia, N.S. Fox, J. Livingstone, Y.J. Shiah, J. Wang, T.A. Beck, C.L. Have, T. Chong, M. Sam, J. Johns, L. Timms, N. Buchner, A. Wong, J.D. Watson, T.T. Simmons, C. P'ng, G. Zafarana, F. Nguyen, X. Luo, K.C. Chu, S.D. Prokopec, J. Sykes, A. Dal Pra, A. Berlin, A. Brown, M.A. Chan-Seng-Yue, F. Yousif, R.E. Denroche, L.C. Chong, G.M. Chen, E. Jung, C. Fung, M.H. Starmans, H. Chen, S.K. Govind, J. Hawley, A. D'Costa, M. Pintilie, D. Waggott, F. Hach, P. Lambin, L.B. Muthuswamy, C. Cooper, R. Eeles, D. Neal, B. Tetu, C. Sahinalp, L.D. Stein, N. Fleshner, S.P. Shah, C.C. Collins, T.J. Hudson, J.D. McPherson, T. van der Kwast, R.G. Bristow, Spatial genomic heterogeneity within localized, multifocal prostate cancer, Nat. Genet. 47 (2015) 736−745.
[12] A.W. Wyatt, M.E. Gleave, Targeting the adaptive molecular landscape of

castration-resistant prostate cancer, EMBO Mol. Med. 7 (2015) 878–894.

[13] H. Beltran, S. Tomlins, A. Aparicio, V. Arora, D. Rickman, G. Ayala, J. Huang, L. True, M.E. Gleave, H. Soule, C. Logothetis, M.A. Rubin, Aggressive variants of castration-resistant prostate cancer, Clin. Canc. Res. : an official journal of the American Association for Cancer Research 20 (2014) 2846–2850.

[14] H. Beltran, D. Prandi, J.M. Mosquera, M. Benelli, L. Puca, J. Cyrta, C. Marotz, E. Giannopoulou, B.V. Chakravarthi, S. Varambally, S.A. Tomlins, D.M. Nanus, S.T. Tagawa, E.M. Van Allen, O. Elemento, A. Sboner, L.A. Garraway, M.A. Rubin, F. Demichelis, Divergent clonal evolution of castration-resistant neuroendocrine prostate cancer, Nat. Med. 22 (2016) 298–305.

[15] H. Beltran, D.S. Rickman, K. Park, S.S. Chae, A. Sboner, T.Y. MacDonald, Y. Wang, K.L. Sheikh, S. Terry, S.T. Tagawa, R. Dhir, J.B. Nelson, A. de la Taille, Y. Allory, M.B. Gerstein, S. Perner, K.J. Pienta, A.M. Chinnaiyan, Y. Wang, C.C. Collins, M.E. Gleave, F. Demichelis, D.M. Nanus, M.A. Rubin, Molecular characterization of neuroendocrine prostate cancer and identification of new drug targets, Canc. Discov. 1 (2011) 487–495.

[16] D. Bernard, A. Pourtier-Manzanedo, J. Gil, D.H. Beach, Myc confers androgen-independent prostate cancer cell growth, JCI (J. Clin. Investig.) 112 (2003) 1724–1731.

[17] J.H. Kim, S.M. Dhanasekaran, R. Mehra, S.A. Tomlins, W. Gu, J. Yu, C. Kumar-Sinha, X. Cao, A. Dash, L. Wang, D. Ghosh, K. Shedden, J.E. Montie, M.A. Rubin, K.J. Pienta, R.B. Shah, A.M. Chinnaiyan, Integrative analysis of genomic aberrations associated with prostate cancer progression, Canc. Res. 67 (2007) 8229–8239.

[18] S.J. Barfeld, A. Urbanucci, H.M. Itkonen, L. Fazli, J.L. Hicks, B. Thiede, P.S. Rennie, S. Yegnasubramanian, A.M. DeMarzo, I.G. Mills, c-Myc antagonises the transcriptional activity of the androgen receptor in prostate cancer affecting key gene networks, EBioMedicine 18 (2017) 83–93.

[19] A.V. Lapuk, S.V. Volik, Y. Wang, C.C. Collins, The role of mRNA splicing in prostate cancer, Asian J. Androl. 16 (2014) 515–521.

[20] N. Nadiminty, R. Tummala, C. Liu, W. Lou, C.P. Evans, A.C. Gao, NF-kappaB2/p52:c-Myc:hnRNPA1 pathway regulates expression of androgen receptor splice variants and enzalutamide sensitivity in prostate cancer, Mol. Canc. Therapeut. 14 (2015) 1884–1895.

[21] R. Hu, C. Lu, E.A. Mostaghel, S. Yegnasubramanian, M. Gurel, C. Tannahill, J. Edwards, W.B. Isaacs, P.S. Nelson, E. Bluemn, S.R. Plymate, J. Luo, Distinct transcriptional programs mediated by the ligand-dependent full-length androgen receptor and its splice variants in castration-resistant prostate cancer, Canc. Res. 72 (2012) 3457–3462.

[22] S. Akamatsu, T. Inoue, O. Ogawa, M.E. Gleave, Clinical and molecular features of treatment-related neuroendocrine prostate cancer, Int. J. Urol. : official journal of the Japanese Urological Association 25 (2018) 345–351.

[23] E.M. Blackwood, R.N. Eisenman, Max: a helix-loop-helix zipper protein that forms a sequence-specific DNA-binding complex with Myc, Science 251 (1991) 1211–1217.

[24] G.J. Kato, W.M. Lee, L.L. Chen, C.V. Dang, Max: functional domains and interaction with c-Myc, Gene Dev. 6 (1992) 81–92.

[25] W.D. Thomas, A. Raif, L. Hansford, G. Marshall, N-myc transcription molecule and oncoprotein, Int. J. Biochem. Cell Biol. 36 (2004) 771–775.

[26] M. Conacci-Sorrell, L. McFerrin, R.N. Eisenman, An overview of MYC and its interactome, Cold Spring Harbor perspectives in medicine 4 (2014) a014357.

[27] J. Michel, R. Cuchillo, The impact of small molecule binding on the energy landscape of the intrinsically disordered protein C-myc, PLoS One 7 (2012), e41070.

[28] F. Jin, C. Yu, L. Lai, Z. Liu, Ligand clouds around protein clouds: a scenario of ligand binding with intrinsically disordered proteins, PLoS Comput. Biol. 9 (2013) e1003249.

[29] C. Yu, X. Niu, F. Jin, Z. Liu, C. Jin, L. Lai, Structure-based inhibitor design for the intrinsically disordered protein c-myc, Sci. Rep. 6 (2016) 22298.

[30] B. Luscher, L.G. Larsson, The basic region/helix-loop-helix/leucine zipper domain of Myc proto-oncoproteins: function and regulation, Oncogene 18 (1999) 2955–2966.

[31] A. Sabo, B. Amati, Genome recognition by MYC, Cold Spring Harbor perspectives in medicine 4 (2014).

[32] P.B. Rahl, R.A. Young, MYC and transcription elongation, Cold Spring Harbor perspectives in medicine 4 (2014), a020990.

[33] A.R. Ferre-D'Amare, G.C. Prendergast, E.B. Ziff, S.K. Burley, Recognition by Max of its cognate DNA through a dimeric b/HLH/Z domain, Nature 363 (1993) 38–45.

[34] S.K. Nair, S.K. Burley, X-ray structures of Myc-Max and Mad-Max recognizing DNA. Molecular bases of regulation by proto-oncogenic transcription factors, Cell 112 (2003) 193–205.

[35] L. Soucek, J. Whitfield, C.P. Martins, A.J. Finch, D.J. Murphy, N.M. Sodir, A.N. Karnezis, L.B. Swigart, S. Nasi, G.I. Evan, Modelling Myc inhibition as a cancer therapy, Nature 455 (2008) 679–683.

[36] L. Soucek, J.R. Whitfield, N.M. Sodir, D. Masso-Valles, E. Serrano, A.N. Karnezis, L.B. Swigart, G.I. Evan, Inhibition of Myc family proteins eradicates KRas-driven lung cancer in mice, Gene Dev. 27 (2013) 504–513.

[37] X. Yin, C. Giap, J.S. Lazo, E.V. Prochownik, Low molecular weight inhibitors of Myc-Max interaction and function, Oncogene 22 (2003) 6151–6159.

[38] J.L. Yap, H. Wang, A. Hu, J. Chauhan, K.Y. Jung, R.B. Gharavi, E.V. Prochownik, S. Fletcher, Pharmacophore identification of c-Myc inhibitor 10074-G5, Bioorg. Med. Chem. Lett 23 (2013) 370–374.

[39] D. Stellas, M. Szabolcs, S. Koul, Z. Li, A. Polyzos, C. Anagnostopoulos, Z. Cournia, C. Tamvakopoulos, A. Klinakis, A. Efstratiadis, Therapeutic effects of an anti-

[40] Myc drug on mouse pancreatic cancer, J. Natl. Cancer Inst. (Bethesda) 106 (2014).

[41] J.R. Hart, A.L. Garner, J. Yu, Y. Ito, M. Sun, L. Ueno, J.K. Rhee, M.M. Baksh, E. Stefan, M. Hartl, K. Bister, P.K. Vogt, K.D. Janda, Inhibitor of MYC identified in a Krohnke pyridine library, Proc. Natl. Acad. Sci. U.S.A. 111 (2014) 12556–12561.

[41] J.R. Whitfield, M.E. Beaulieu, L. Soucek, Strategies to inhibit myc and their clinical applicability, Frontiers in cell and developmental biology 5 (2017) 10.

[42] C.M. Koh, A. Sabo, E. Guccione, Targeting MYC in cancer therapy: RNA processing offers new opportunities, Bioessays : news and reviews in molecular, cellular and developmental biology 38 (2016) 266–275.

[43] M.R. McKeown, J.E. Bradner, Therapeutic strategies to inhibit MYC, Cold Spring Harbor perspectives in medicine 4 (2014).

[44] D.S. Rickman, J.H. Schulte, M. Eilers, The expanding world of N-MYC-Driven tumors, Canc. Discov. 8 (2018) 150–163.

[45] A.V. Follis, D.I. Hammoudeh, H. Wang, E.V. Prochownik, S.J. Metallo, Structural rationale for the coupled binding and unfolding of the c-Myc oncoprotein by small molecules, Chem. Biol. 15 (2008) 1149–1155.

[46] D.I. Hammoudeh, A.V. Follis, E.V. Prochownik, S.J. Metallo, Multiple independent binding sites for small-molecule inhibitors on the oncoprotein c-Myc, J. Am. Chem. Soc. 131 (2009) 7390–7401.

[47] H. Wang, D.I. Hammoudeh, A.V. Follis, B.E. Reese, J.S. Lazo, S.J. Metallo, E.V. Prochownik, Improved low molecular weight Myc-Max inhibitors, Mol. Canc. Therapeut. 6 (2007) 2399–2408.

[48] H. Wang, J. Chauhan, A. Hu, K. Pendleton, J.L. Yap, P.E. Sabato, J.W. Jones, M. Perri, J. Yu, E. Cione, M.A. Kane, S. Fletcher, E.V. Prochownik, Disruption of Myc-Max heterodimerization with improved cell-penetrating analogs of the small molecule 10074-G5, Oncotarget 4 (2013) 936–947.

[49] J. Guo, R.A. Parise, E. Joseph, M.J. Egorin, J.S. Lazo, E.V. Prochownik, J.L. Eiseman, Efficacy, pharmacokinetics, tisssue distribution, and metabolism of the Myc-Max disruptor, 10058-F4 [Z,E]-5-[4-ethylbenzylidine]-2-thioxothiazolidin-4-one, in mice, Canc. Chemother. Pharmacol. 63 (2009) 615–625.

[50] D.M. Clausen, J. Guo, R.A. Parise, J.H. Beumer, M.J. Egorin, J.S. Lazo, E.V. Prochownik, J.L. Eiseman, In vitro cytotoxicity and in vivo efficacy, pharmacokinetics, and metabolism of 10074-G5, a novel small-molecule inhibitor of c-Myc/Max dimerization, J. Pharmacol. Exp. Therapeut. 335 (2010) 715–727.

[51] Molecular Operating Environment (MOE), 2013.08; Chemical Computing Group ULC, 1010 Sherbooke St. West, Suite #910, Montreal, QC, Canada, H3A 2R7, 2018.

[52] L.A. Jung, A. Gebhardt, W. Koelmel, C.P. Ade, S. Walz, J. Kuper, B. von Eyss, S. Letschert, C. Redel, L. d'Artista, A. Biankin, L. Zender, M. Sauer, E. Wolf, G. Evan, C. Kisker, M. Eilers, OmoMYC blunts promoter invasion by oncogenic MYC to inhibit gene expression characteristic of MYC-dependent tumors, Oncogene 36 (2017) 1911–1924.

[53] J.J. Irwin, B.K. Shoichet, ZINC–a free database of commercially available compounds for virtual screening, J. Chem. Inf. Model. 45 (2005) 177–182.

[54] J.J. Irwin, T. Sterling, M.M. Mysinger, E.S. Bolstad, R.G. Coleman, ZINC: a free tool to discover chemistry for biology, J. Chem. Inf. Model. 52 (2012) 1757–1768.

[55] R.A. Friesner, J.L. Banks, R.B. Murphy, T.A. Halgren, J.J. Klicic, D.T. Mainz, M.P. Repasky, E.H. Knoll, M. Shelley, J.K. Perry, D.E. Shaw, P. Francis, P.S. Shenkin, Glide: a new approach for rapid, accurate docking and scoring. 1. Method and assessment of docking accuracy, J. Med. Chem. 47 (2004) 1739–1749.

[56] T.A. Halgren, R.B. Murphy, R.A. Friesner, H.S. Beard, L.L. Frye, W.T. Pollard, J.L. Banks, Glide: a new approach for rapid, accurate docking and scoring. 2. Enrichment factors in database screening, J. Med. Chem. 47 (2004) 1750–1759.

[57] Schrödinger Release 2018-1, Maestro, Schrödinger, LLC, New York, NY, 2018.

[58] M.J. Huang, Y.C. Cheng, C.R. Liu, S. Lin, H.E. Liu, A small-molecule c-Myc inhibitor, 10058-F4, induces cell-cycle arrest, apoptosis, and myeloid differentiation of human acute myeloid leukemia, Exp. Hematol. 34 (2006) 1480–1489.

[59] N. Lallous, K. Dalal, A. Cherkasov, P.S. Rennie, Targeting alternative sites on the androgen receptor to treat castration-resistant prostate cancer, Int. J. Mol. Sci. 14 (2013) 12496–12519.

[60] P. Axerio-Cilies, N.A. Lack, M.R. Nayana, K.H. Chan, A. Yeung, E. Leblanc, E.S. Guns, P.S. Rennie, A. Cherkasov, Inhibitors of androgen receptor activation function-2 (AF2) site identified through virtual screening, J. Med. Chem. 54 (2011) 6197–6205.

[61] N.A. Lack, P. Axerio-Cilies, P. Tavassoli, F.Q. Han, K.H. Chan, C. Feau, E. LeBlanc, E.T. Guns, R.K. Guy, P.S. Rennie, A. Cherkasov, Targeting the binding function 3 (BF3) site of the human androgen receptor through virtual screening, J. Med. Chem. 54 (2011) 8563–8573.

[62] R.S. Munuganti, E. Leblanc, P. Axerio-Cilies, C. Labriere, K. Frewin, K. Singh, M.D. Hassona, N.A. Lack, H. Li, F. Ban, E. Tomlinson Guns, R. Young, P.S. Rennie, A. Cherkasov, Targeting the binding function 3 (BF3) site of the androgen receptor through virtual screening. 2. development of 2-((2-phenoxyethyl) thio)-1H-benzimidazole derivatives, J. Med. Chem. 56 (2013) 1136–1148.

[63] R.S. Munuganti, M.D. Hassona, E. Leblanc, K. Frewin, K. Singh, D. Ma, F. Ban, M. Hsing, H. Adomat, N. Lallous, C. Andre, J.P. Jonadass, A. Zoubeidi, R.N. Young, E.T. Guns, P.S. Rennie, A. Cherkasov, Identification of a potent antiandrogen that targets the BF3 site of the androgen receptor and inhibits

enzalutamide-resistant prostate cancer, Chem. Biol. 21 (2014) 1476—1485.

[64] F. Ban, E. Leblanc, H. Li, R.S. Munuganti, K. Frewin, P.S. Rennie, A. Cherkasov, Discovery of 1H-indole-2-carboxamides as novel inhibitors of the androgen receptor binding function 3 (BF3), J. Med. Chem. 57 (2014) 6867—6872.

[65] H. Li, M.D. Hassona, N.A. Lack, P. Axerio-Cilies, E. Leblanc, P. Tavassoli, N. Kanaan, K. Frewin, K. Singh, H. Adomat, K.J. Bohm, H. Prinz, E.T. Guns, P.S. Rennie, A. Cherkasov, Characterization of a new class of androgen receptor antagonists with potential therapeutic application in advanced prostate cancer, Mol. Canc. Therapeut. 12 (2013) 2425—2435.

[66] H. Li, F. Ban, K. Dalal, E. Leblanc, K. Frewin, D. Ma, H. Adomat, P.S. Rennie, A. Cherkasov, Discovery of small-molecule inhibitors selectively targeting the DNA-binding domain of the human androgen receptor, J. Med. Chem. 57 (2014) 6458—6467.

[67] K. Dalal, M. Roshan-Moniri, A. Sharma, H. Li, F. Ban, M.D. Hassona, M. Hsing, K. Singh, E. LeBlanc, S. Dehm, E.S. Tomlinson Guns, A. Cherkasov, P.S. Rennie, Selectively targeting the DNA-binding domain of the androgen receptor as a prospective therapy for prostate cancer, J. Biol. Chem. 289 (2014) 26417—26429.

[68] P.C. Hawkins, A.G. Skillman, A. Nicholls, Comparison of shape-matching and docking as virtual screening tools, J. Med. Chem. 50 (2007) 74—82.

[69] OpenEye Scientific Software, Santa Fe, NM. http://www.eyesopen.com (last accessed May, 2018).

[70] T. Sterling, J.J. Irwin, ZINC 15–ligand discovery for everyone, J. Chem. Inf. Model. 55 (2015) 2324—2337.

[71] P.C. Hawkins, A.G. Skillman, G.L. Warren, B.A. Ellingson, M.T. Stahl, Conformer generation with OMEGA: algorithm and validation using high quality structures from the Protein Databank and Cambridge Structural Database, J. Chem. Inf. Model. 50 (2010) 572—584.

[72] M.A. Neves, M. Totrov, R. Abagyan, Docking and scoring with ICM: the benchmarking results and strategies for improvement, J. Comput. Aided Mol. Des. 26 (2012) 675—686.

[73] M. McGann, FRED pose prediction and virtual screening accuracy, J. Chem. Inf. Model. 51 (2011) 578—596.

[74] M. McGann, FRED and HYBRID docking performance on standardized datasets, J. Comput. Aided Mol. Des. 26 (2012) 897—906.

[75] mol_rmsd Calculate RMSD's for docking results, Scientific Vector Language (SVL) source code provided by Chemical Computing Group ULC, 1010 Sherbrooke St. West, Suite #910, Montreal, QC, Canada, H3A 2R7, 2018.

[76] Scoring Analysis tool for non-bonded intermolecular interactions: H-bonds, transition metal, water bridges, hydrophobic, Scientific Vector Language (SVL) source code provided by Chemical Computing Group ULC, 1010 Sherbrooke St. West, Suite #910, Montreal, QC, Canada, H3A 2R7, 2018.

[77] A. Cherkasov, E.N. Muratov, D. Fourches, A. Varnek, Baskin II, M. Cronin, J. Dearden, P. Gramatica, Y.C. Martin, R. Todeschini, V. Consonni, V.E. Kuz'min, R. Cramer, R. Benigni, C. Yang, J. Rathman, L. Terfloth, J. Gasteiger, A. Richard, A. Tropsha, QSAR modeling: where have you been? Where are you going to?

[78] N. Paul, L.A. Carabet, N. Lallous, T. Yamazaki, M.E. Gleave, P.S. Rennie, A. Cherkasov, Cheminformatics modeling of adverse drug responses by clinically relevant mutants of human androgen receptor, J. Chem. Inf. Model. 56 (2016) 2507—2516.

[79] F. Ban, K. Dalal, H. Li, E. LeBlanc, P.S. Rennie, A. Cherkasov, Best practices of computer-aided drug discovery: lessons learned from the development of a preclinical candidate for prostate cancer with a new mechanism of action, J. Chem. Inf. Model. 57 (2017) 1018—1028.

[80] Schrödinger Release 2018-1, FEP+, Schrödinger, New York, NY, 2018.

[81] R. Abel, L. Wang, E.D. Harder, B.J. Berne, R.A. Friesner, Advancing drug discovery through enhanced free energy calculations, Accounts Chem. Res. 50 (2017) 1625—1632.

[82] B. Kuhn, M. Tichy, L. Wang, S. Robinson, R.E. Martin, A. Kuglstatter, J. Benz, M. Giroud, T. Schirmeister, R. Abel, F. Diederich, J. Hert, Prospective evaluation of free energy calculations for the prioritization of cathepsin L inhibitors, J. Med. Chem. 60 (2017) 2485—2497.

[83] L. Wang, Y. Deng, Y. Wu, B. Kim, D.N. LeBard, D. Wandschneider, M. Beachy, R.A. Friesner, R. Abel, Modeling of scaffold hopping transformations in drug discovery, J. Chem. Theor. Comput. 13 (2017) 42—54.

[84] E. Harder, W. Damm, J. Maple, C. Wu, M. Reboul, J.Y. Xiang, L. Wang, D. Lupyan, M.K. Dahlgren, J.L. Knight, J.W. Kaus, D.S. Cerutti, G. Krilov, W.L. Jorgensen, R. Abel, R.A. Friesner, OPLS3: a force field providing broad coverage of drug-like small molecules and proteins, J. Chem. Theor. Comput. 12 (2016) 281—296.

[85] L. Wang, Y. Wu, Y. Deng, B. Kim, L. Pierce, G. Krilov, D. Lupyan, S. Robinson, M.K. Dahlgren, J. Greenwood, D.L. Romero, C. Masse, J.L. Knight, T. Steinbrecher, T. Beuming, W. Damm, E. Harder, W. Sherman, M. Brewer, R. Wester, M. Murcko, L. Frye, R. Farid, T. Lin, D.L. Mobley, W.L. Jorgensen, B.J. Berne, R.A. Friesner, R. Abel, Accurate and reliable prediction of relative ligand binding potency in prospective drug discovery by way of a modern free-energy calculation protocol and force field, J. Am. Chem. Soc. 137 (2015) 2695—2703.

[86] ADMET Predictor 8.5. http://www.simulations-plus.com/software/admetpredictor/(last accessed May, 2018).

[87] A. Castell, Q. Yan, K. Fawkner, P. Hydbring, F. Zhang, V. Verschut, M. Franco, S.M. Zakaria, W. Bazzar, J. Goodwin, G. Zinzalla, L.-G. Larsson, A selective high affinity MYC-binding compound inhibits MYC:MAX interaction and MYC-dependent tumor cell proliferation, Sci. Rep. 8 (2018) 10064.

[88] G.M. Sastry, M. Adzhigirey, T. Day, R. Annabhimoju, W. Sherman, Protein and ligand preparation: parameters, protocols, and influence on virtual screening enrichments, J. Comput. Aided Mol. Des. 27 (2013) 221—234.

[89] Schrödinger Release 2018-1, Schrödinger Suite 2018-1 Protein Preparation Wizard, Impact, Schrödinger, LLC, New York, NY, 2016; Prime, Schrödinger, LLC, New York, NY, 2018, Epik, Schrödinger, LLC, New York, NY, 2016.